Impurity spin resonance and spin-cluster resonance in $(CH_3)_3NHCo_{1-x}Mn_xCl_3 \cdot 2H_2O$

A. C. Phaff, C. H. W. Swüste, and W. J. M. de Jonge
Department of Physics, Eindhoven University of Technology, Eindhoven, The Netherlands
(Received 18 December 1981)

Resonance of manganese impurities in the quasi-one-dimensional Ising-like magnetic system $(CH_3)_3NHCoCl_3 \cdot 2H_2O$ has been observed in the frequency-field region 18–58 GHz, 0–7 T, whereas in this same region resonance of copper impurities could not be discovered. Detailed analysis of the manganese resonance spectrum will provide information about the strength and nature of the Mn-Co interaction. Resonances of the cobalt hosts were also observed; these resonances are of the spin-cluster type and therefore contain information about the Co-Co interchain exchange interaction.

I. INTRODUCTION

Recently there has been growing interest in the behavior of three-dimensional ordering of quasi-one-dimensional magnetic systems upon dilution with nonmagnetic or weakly magnetic impurities.[1,2] This ordering process is particularly sensitive to impurities because of the hampering effect these may have on the development of correlations between the magnetic moments in the one-dimensional magnetic chains. Hone *et al.*[2] showed that an Ising system, as compared with a Heisenberg system, should be very sensitive to impurities, and therefore an Ising system would be an appropriate candidate for testing their theoretical predictions.

For this reason Takeda[3] performed specific-heat measurements on the Ising-like compound $(CH_3)_3NHCoCl_3 \cdot 2H_2O$ diluted with Mn^{2+} ions, whereas Schouten *et al.*[1,4] did the same kind of measurements on $(CH_3)_3NHCoCl_3 \cdot 2H_2O$ diluted with Cu^{2+} ions. From the maximum of the specific-heat anomalies they determined the values of the three-dimensional (3D) ordering termperature T_N in dependence on the impurity concentration x, for x up to about 0.25.

Comparison of their results reveals striking differences in magnitude as well as in behavior of $T_N(x)/T_N(0)$ vs x, as can be seen in Fig. 1. The results of Takeda and Schouten could be explained within the framework of the theory of Hone if one assumes the manganese impurities to act as weakly magnetic and the copper impurities as strongly magnetic. To see whether or not these assumptions are correct we decided to study the impurity-host interaction parameters in more detail by means of spectroscopic measurements in the range 18–58 GHz.

This method of investigation of impurity-host interaction by spectroscopic measurements (impurity spin resonance) has been rather successful during the last two decades. Examples which have some similarity to the work reported here are: Fe^{3+} in $FeCl_2$ by Date *et al.*,[5] Mn^{2+} and Fe^{3+} in $FeCl_2$ by Motokawa *et al.*,[6] Mn^{2+} in $CoCl_2 \cdot 2H_2O$ by Fujii *et al.*,[7] Er^{3+} in MnF_2 by Chase *et al.*,[8] and more recently Mn^{2+} in $FeBr_2$ by Mischler *et al.*[9] and Mn^{2+} in $FeCl_2$ by Tuchendler *et al.*[10]

Apart from investigation of impurity-host interaction by means of impurity spin resonance it is also possible to study simultaneously the host-host interchain interaction by means of spin-cluster resonance.[11,12] These spin-cluster resonances can be distinguished from the impurity spin resonances through, for instance, a totally different temperature dependence.

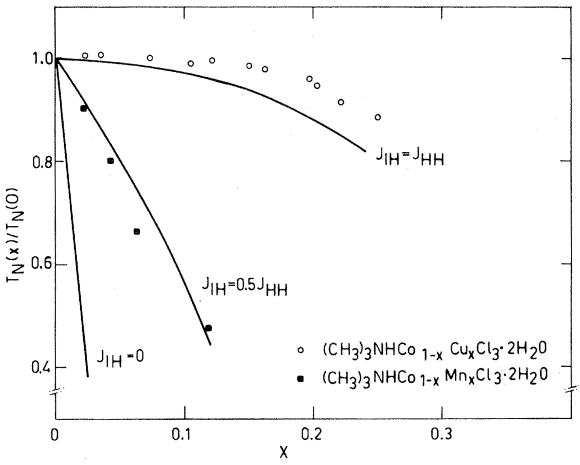

FIG. 1. The reduced ordering temperature $T_N(x)/T_N(0)$ as a function of x. The solid lines represent the theoretical predictions for a quasi-one-dimensional Ising system for various values of J_{IH}/J_{HH}. (I = impurity, H = host.) The squares are the values of Takeda (Ref. 3) for Mn^{2+} impurities and the circles are the values of Schouten (Ref. 1) for Cu^{2+} impurities.

The organization of this paper is as follows: in Sec. II we give the crystallographic and magnetic properties of $(CH_3)_3NHCoCl_3 \cdot 2H_2O$. Section III describes the experimental circumstances. Section IV will deal with the impurity spin resonance and Sec. V with the spin-cluster-type resonances. Finally in Sec. VI we try to gain some physical insight by discussing the results of the previous sections.

II. CRYSTALLOGRAPHIC AND MAGNETIC PROPERTIES OF $(CH_3)_3NHCoCl_3 \cdot 2H_2O$

$(CH_3)_3NHCoCl_3 \cdot 2H_2O$ belongs to the series of isomorphic hydrated trimethyl ammonium halides $(CH_3)_3NHMB_3 \cdot 2H_2O$, with metal ion M being Co, or Mn, or Cu and B = Cl or Br. All members of this series show more of less pronounced linear-chain characteristics.[13–17]

The crystallographic structure of $(CH_3)_3NHCoCl_3 \cdot 2H_2O$ was determined by Losee *et al.*[13] as being orthorhombic with space group *Pnma*. The structure consists of chains of edge sharing *trans*-$[CoCl_4(OH_2)_2]$ octahedra running parallel to the b axis, the two Cl^- ions on the shared edges thus providing a strong superexchange path. The chains are linked weakly in the c direction by hydrogen bridges, whereas in the a direction they are seperated by bulky trimethyl ammonium groups and the third chlorine ion.

Single crystals of $(CH_3)_3NHCoCl_3 \cdot 2H_2O$ are obtained by slow evaporation at room temperature from an aqueous solution of equimolar amounts of $(CH_3)_3NHCl$ and $CoCl_2 \cdot 6H_2O$. The mixed crystals could easily be grown from a solution of equimolar amounts of $(CH_3)_3NHCl$ and $Co_{1-x}M_xCl_2 \cdot 6H_2O$ (M = Cu or Mn). The crystals grow as prisms elongated along the b axis with typical dimensions of $2 \times 2 \times 7$ mm^3. The molar concentration of impurity ions in the crystals was checked by commercial chemical analysis and systematically was about twice the molar concentration of impurity ions in the solutions.

From specific-heat and susceptibility measurements by Losee *et al.*[13] it was deduced that $(CH_3)_3NHCoCl_3 \cdot 2H_2O$ consists of Ising-like ferromagnetic chains with intrachain exchange interaction $J/k = 15.4$ K and an antiferromagnetic interchain interaction with $J'/k = -0.18$ K. The system orders at $T_N = 4.135$ K.

The magnetic structure was determined by Spence *et al.*[18] by means of NMR and magnetization measurements as *Pnm'a'*. Figure 2(a) shows a picture of the spin structure in the "antiferromagnetic phase." The spins lie in the a-c plane and show a canting of about 10° with respect to the c axis, giving rise to a noncompensated ferromagnetic component along the a axis. With a magnetic field along the c axis the system exhibits a metamagnetic phase transition at 64 Oe, which has a width that is determined by the demagnetizing field and may be as large as 500 Oe. In this region the system is in a mixed "antiferromagnetic"-"ferromagnetic" state with domains. At fields above a certain value (Groenendijk *et al.*[19]) the system is fully magnetized and in a ferromagnetic state with spin structure as shown in Fig. 2(b).

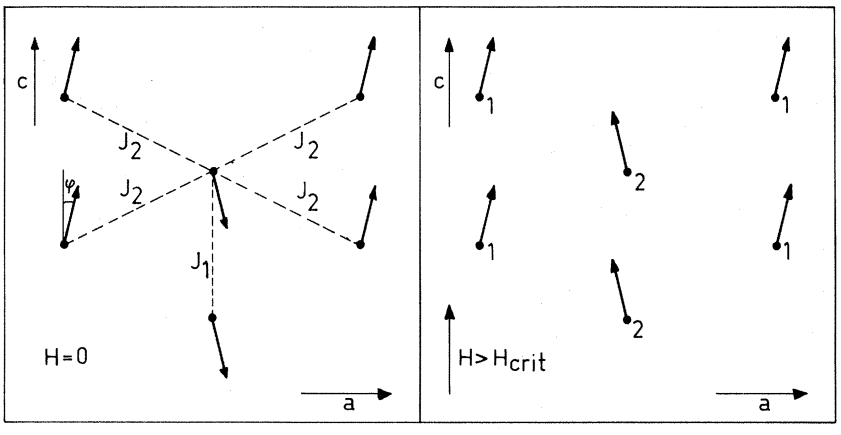

(a) (b)

FIG. 2. (a) Spin structure in the antiferromagnetic ground state (β phase). The interaction J_1 couples the spins into layers in the b-c plane. The interaction J_2 very loosely couples these layers. The canting angle ϕ is about 10°. (b) The field-induced ferromagnetic spin structure (α phase). This configuration starts to be realized for $H > H_c = 64$ Oe.

III. EXPERIMENTAL

The measurements were done using conventional microwave spectrometers covering the range 18–58 GHz.[20] The samples were placed at the end of a closed waveguide that was immersed in liquid helium. In some cases this waveguide was equipped with a device that enabled us to rotate the sample along an axis perpendicular to the magnetic field.

By pumping the liquid-helium bath, temperatures between 1.2 and 4.2 K could be reached. A rotatable but small (up to 1 T) magnetic field was supplied by a conventional iron electromagnet; higher fields (not rotatable), up to 7 T, could be obtained from a superconducting solenoid.

Experiments with rotating sample were done with the field in the crystallographic a-c plane, whereas the experiments with static field or static sample were carried out with the field along the a or c axis. For some measurements where we needed higher spectrometer sensitivity we used a more elaborate Varian spectrometer that was equipped with a 35-GHz cavity; however, in this setup the field was limited to 1 T.

Measurements were done on a multitude of samples, among which were Cu-doped samples with impurity concentrations x of 0.039, 0.058, 0.156, 0.222; Mn-doped samples with impurity concentrations 0.005, 0.011, 0.020, 0.031; and one pure sample.

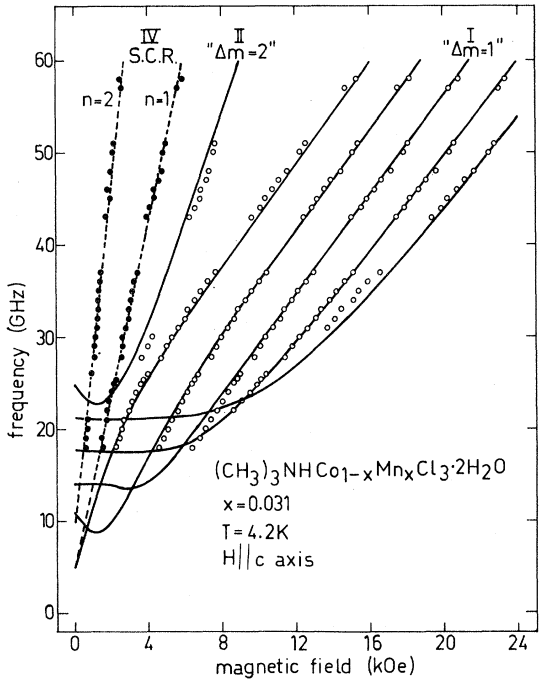

FIG. 3. Frequency-field diagram of the ISR and the SCR for $T=4.2$ K and $\vec{H} \| c$. The open circles represent impurity spin resonances and the solid circles represent spin-cluster resonances. The solid and dashed lines are fits to the data using the expressions and parameters given in the text.

IV. IMPURITY SPIN RESONANCE (ISR)

A. Resonance of manganese impurities

Figures 3 and 4 show typical resonance data of $(CH_3)_3NHCo_{1-x}Mn_xCl_3 \cdot 2H_2O$ with $x=0.031$. Our measurements on this compound have been performed at temperatures of 4.2 and 1.3 K, that is well above and well below the 3D-ordering temperature of about 3.6 K as determined by Takeda.[3]

The resonance data at 4.2 and 1.3 K are quite similar with respect to the line positions, which indicates that the magnetic field induces the same ferromagnetic phase both at 4.2 and 1.3 K. However, the relative line intensities are, of course, affected by changing the temperature. Figure 3 is a representative of a frequency-field diagram of the resonances at 4.2 K with $\vec{H} \| c$ whereas Fig. 4 is representative for a frequency-field diagram of the resonances at 1.3 K with $\vec{H} \| a$. The main feature of both these resonance spectra is a set of five strong resonance lines (indicated by I) which at high fields tend to run parallel.

We also measured the angular dependence of the resonance spectrum on rotating the magnetic field in the a-c plane. Figure 5 shows a rotation diagram at a frequency of 50.5 GHz and a temperature of 4.2 K. In this diagram we can distinguish three regions, denoted by α, B, and β.[18] These regions indicate the

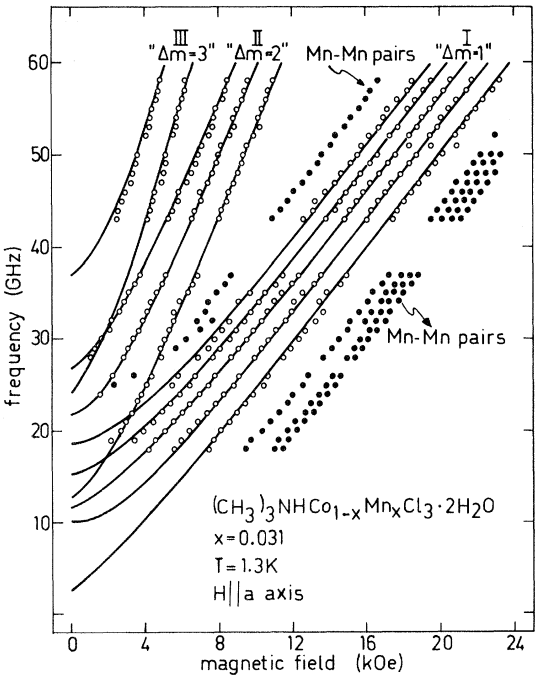

FIG. 4. Frequency-field diagram of the ISR for $T=1.3$ K and $\vec{H} \| a$. The open circles represent resonances of single impurity spins whereas the solid circles represent excitations of impurity spin pairs. The drawn curves are calculated using the Hamiltonian (3) and the parameters given in the text.

magnetic ordering of the pure host: in region α the ordering is ferromagnetic [Fig. 2(b)] and M_c is saturated; in region β the ordering is antiferromagnetic [Fig. 2(a)] and M_a is saturated; in region B the pure host is in a mixed phase with domains of ferromagnetic as well as antiferromagnetic ordering.[19]

We see that each of the resonance lines in Fig. 5 splits up if the field is rotated away from the c axis, which illustrates the fact that half of the manganese ions are in chains with direction 1 and half in chains with direction 2 (see Fig. 2). Here the direction of a chain is to be understood as the direction of the ferromagnetic moment of the chain.

All the features of the spectra of Figs. 3, 4, and 5 can be understood assuming the Hamiltonian of a manganese impurity to be of the form

$$\mathcal{H}_i = \mu_B \vec{S} \cdot \vec{g}_i \cdot \vec{H}_i + \vec{S} \cdot \vec{D}_i \cdot \vec{S} \ . \tag{1}$$

(Strictly speaking, the field should be written B, but in practice H is generally used.[21]) Here the subscript i denotes to which Co chain ($i=1$ or $i=2$) the manganese ion belongs. $\vec{H}_i$ is the sum of the external field $\vec{H}_{\text{ext}}$ and the internal field $\vec{H}_{i,\text{int}}$

$$\vec{H}_i = \vec{H}_{\text{ext}} + \vec{H}_{i,\text{int}} \ . \tag{2}$$

$\vec{H}_{i,\text{int}}$ is thought to be composed of two contributions, one that takes into account the impurity-host exchange interaction and a contribution of dipolar origin.

The tensors $\vec{g}_i$ and $\vec{D}_i$ are assumed to be diagonal in (x_i, y_i, z_i) for $i=1,2$. The directions of the z_1 and z_2 axes are supposed to be parallel to the two possible directions of the Co moments (see Fig. 6), whereas the y_1 and y_2 axes are along the chain direction (b axis). If we take our z axis along z_1 or z_2 and y along b and assume $g_x = g_y$ then the Hamiltonian (1) can be written

$$\mathcal{H} = \mu_B g_{\parallel} S_z H_z + \mu_B g_{\perp} (S_x H_x + S_y H_y) + E(S_x^2 - S_y^2) + D[S_z^2 - \tfrac{1}{3} S(S+1)] \tag{3}$$

with $S = \frac{5}{2}$.

The term $-\frac{1}{3} DS(S+1)$ has been added to make $\mathcal{H}$ traceless. For each value of H the Hamiltonian (3) has six eigenvalues E_j with $E_j > E_k$ for $j > k$.

The dominating feature of the frequency-field diagrams are the bundles of five resonance lines, designated by I in Figs. 3 and 4; these lines are due to transitions between adjacent energy levels, $E_j \rightarrow E_{j+1}$. It can be shown that transitions between nonadjacent energy levels have a small but certainly not negligible transition probability. In fact, the lines designated by II and III, which are on the average 25 times weaker than those of type I, are transitions between nonadja-

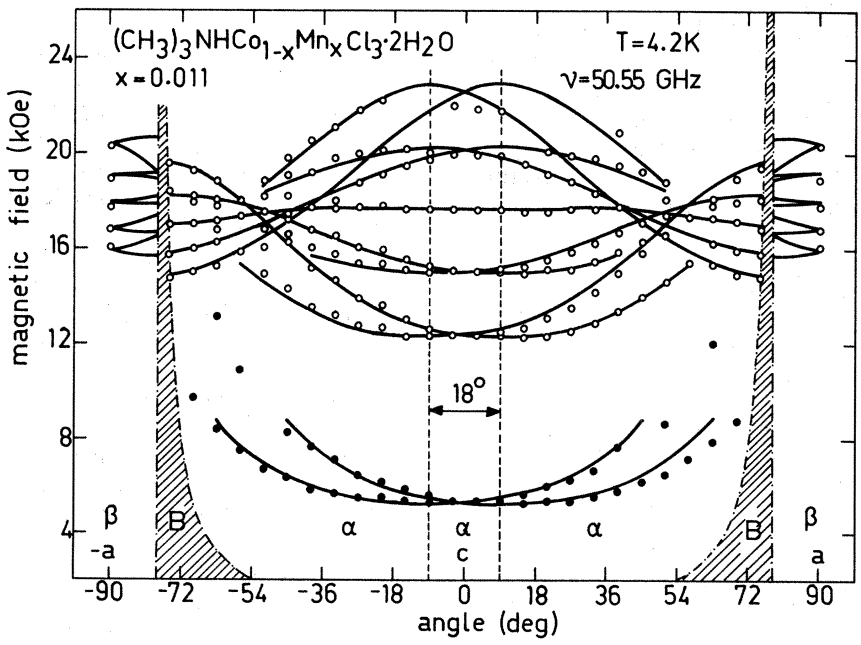

FIG. 5. Rotation diagram of the ISR and the SCR at a fixed frequency of 50.5 GHz. In region α the spin structure is ferromagnetic, in β antiferromagnetic, and region B is a mixture of both these structures. The open circles represent the ISR, whereas the solid circles represent the SCR. The drawn curves are calculated using the expressions and parameters given in the text.

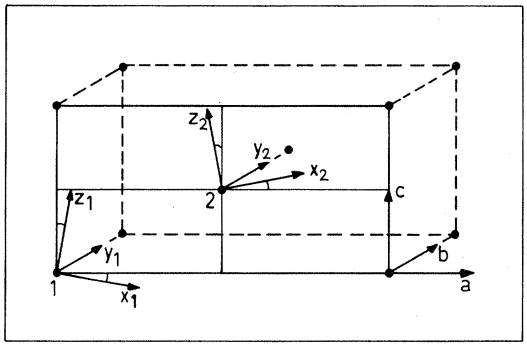

FIG. 6. The local frames of reference at the two possible impurity positions 1 and 2. The angle between z_i and c is about 10°.

cent energy levels; the lines II are transitions between levels separated by one level, $E_j \rightarrow E_{j+2}$, and the lines III are transitions between levels separated by two levels, $E_j \rightarrow E_{j+3}$. In principle there should be four lines of type II and three lines of type III; we only see three of type II and two of type III, the others apparently too weak to be seen. In the high-field limit the resonance lines I, II, and III correspond to changes in the magnetic quantum number m of, respectively, 1, 2, and 3; therefore these lines are also labeled "$\Delta m = 1$," "$\Delta m = 2$," and "$\Delta m = 3$."

So far we have not considered the intensity of the resonance lines, however, the relative line intensities are very useful in interpreting the data because these contain information about (i) the transition probability, (ii) the occupation of the energy levels, and (iii) the relaxation rate. For example, the sign of D is obtained from comparing the line intensities of the lines I with a theoretical expression for item (ii).

The resonance data in Fig. 3, 4, and 5 can be fitted by the Hamiltonian (3) if we use the following parameters:

$D = -3.85$ GHz (-0.128 cm^{-1}) ± 0.1 GHz ,

$E = -0.27$ GHz (-0.009 cm^{-1}) ± 0.03 GHz ,

$g_{\parallel} = 1.93 \pm 0.01$, $g_{\perp} = 1.86 \pm 0.01$,

angle between z_1 and $c = 9° \pm 1°$,

angle between z_2 and $c = -9° \pm 1°$,

x component of $\vec{H}_{int}$ ($\vec{H} \parallel c$) $= 0 \pm 0.5$ kOe,

y component of $\vec{H}_{int}$ ($\vec{H} \parallel c$) $= 5.0 \pm 0.5$ kOe,

z component of $\vec{H}_{int}$ ($\vec{H} \parallel c$) $= 0.5 \pm 0.2$ kOe (Fig. 3);

x component of $\vec{H}_{int}$ ($\vec{H} \parallel a$) $= 0.9 \pm 0.2$ kOe,

y component of $\vec{H}_{int}$ ($\vec{H} \parallel a$) $= 4.0 \pm 0.5$ kOe,

z component of $\vec{H}_{int}$ ($\vec{H} \parallel a$) $= 0 \pm 0.5$ kOe (Fig. 4).

These parameter values and the uncertainties of these values are obtained by a method of trial and error. We see that the main component of $\vec{H}_{int}$ is the y component, the x and z components being much smaller and depending on the direction of the external field and also on the sample shape. In order to estimate the exchange contribution to $\vec{H}_{int}$ we calculated the dipolar fields at the manganese positions for a spherical sample. This dipolar field lies in the x-z plane and is directed almost opposite to the Co^{2+} moments, the magnitude being 1.2 kOe in the α region and 0.7 kOe in the β region. The exchange part of $\vec{H}_{int}$ is obtained by subtraction of this dipolar field from $\vec{H}_{int}$, therefore the y component of $\vec{H}_{int}$ is of exchange origin and the exchange contributions to the x and z component are much smaller than the y component. Summarizing, we may state that $\vec{H}_{int}$ is mainly of exchange origin, is directed along the chain direction, and has a magnitude of about 4.5 kOe. The origin of this exchange field will be discussed in Sec. VI.

Another interesting aspect of Fig. 4 are the weak resonances to the right and to the left side of set I (the black dots), which in intensity are comparable with the resonances of types II and III. These resonances may be brought about by Mn^{2+}-Mn^{2+} pairs in a similar way as described by Tuchendler *et al.*[10] for $Fe_{1-x}Mn_xCl_2$. In order to check the origin of these resonances we performed measurements on a sample with an impurity concentration $x = 0.011$, where the density of Mn^{2+}-Mn^{2+} pairs should be about nine times as low as in a sample with $x = 0.031$. So in the sample with $x = 0.031$ the ratio of the pair line intensities to the intensities of the lines I is expected to be nine times as high as in the sample with $x = 0.011$. Unfortunately this test was sabotaged by hyperfine splitting of the lines I, that prevented us from a precise determination of intensity ratios.

Nevertheless, a rough estimate shows that this ratio for $x = 0.011$ is much smaller than in the case $x = 0.031$, confirming that we indeed are dealing with Mn^{2+}-Mn^{2+} pairs. Just to illustrate the effects of Mn^{2+}-Mn^{2+} pairs and hyperfine splitting, we depicted in Fig. 7 two signal traces: one for $x = 0.031$ [Fig. 7(a)] and one for $x = 0.011$ [Fig. 7(b)]. We can expect a pair exchange interaction of roughly the same magnitude as the intrachain interaction in $(CH_3)_3NHMnCl_3 \cdot 2H_2O$ which is $J/k = -0.36$ K (Ref. 15). The Zeeman energy and the exchange energy of the pair with its cobalt neighbors also have this order of magnitude, making it difficult to approach the pair problem with perturbation methods. Therefore we were not able to identify unambiguously the pair resonances with transitions in the pair energy level scheme and could not determine the parameters of the pair Hamiltonian.

Now there are only the lines IV in Fig. 3 and the two lower lines (black dots) in Fig. 5 left to be explained. These lines have a completely different origin and have nothing to do with the impurity ions,

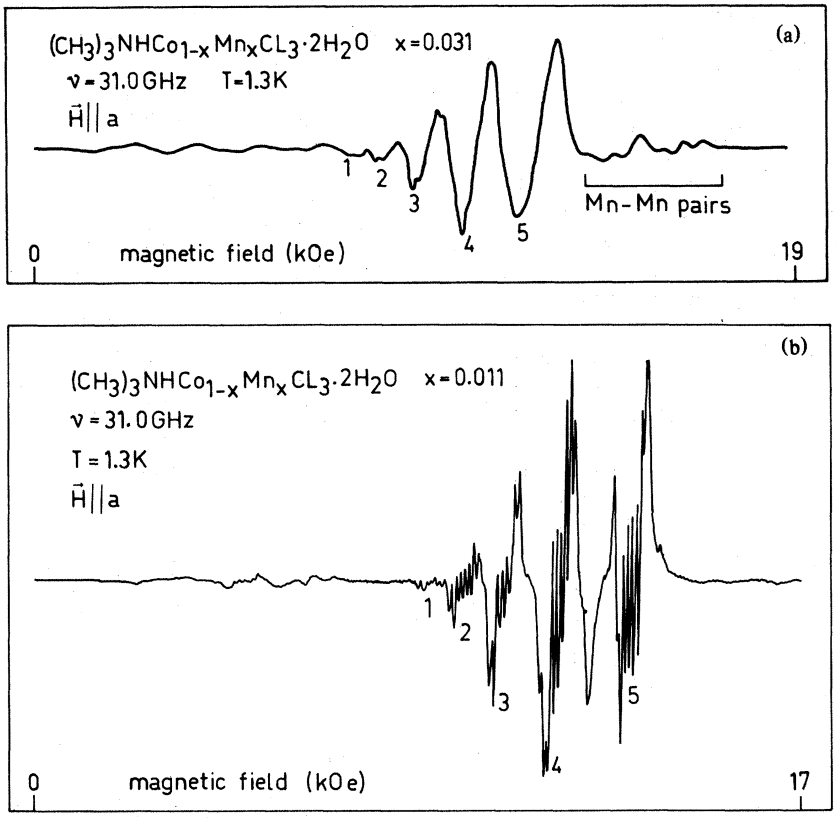

FIG. 7. (a) Signal trace for a sample with $x=0.031$. Along the vertical axes is the first derivative of the microwave absorption in arbitrary units. The five fine-structure lines (1,2,3,4,5) show some distortion caused by a tendency towards hyperfine splitting. Signals arising from Mn^{2+}-Mn^{2+} pairs are clearly visible. (b) Signal trace for a sample with $x=0.011$. The five fine-structure lines are split by hyperfine interaction. The signals arising from Mn^{2+}-Mn^{2+} pairs have almost disappeared for this impurity concentration. Note that the magnetic field scales in (a) and (b) are somewhat different.

for these can also be seen in pure $(CH_3)_3NHCoCl_3\cdot 2H_2O$ as well as in $(CH_3)_3NHCo_{1-x}Cu_xCl_3\cdot 2H_2O$ and so they must find their origin in the Co^{2+}-host ions.

Section V will deal with these resonances.

B. Resonance of copper impurities

In order to investigate the Cu^{2+}-Co^{2+} interaction we searched for Cu^{2+} resonances in $(CH_3)_3NHCo_{1-x}Cu_xCl_3\cdot 2H_2O$ in exactly the same way as we searched for Mn^{2+} resonances in $(CH_3)_3NHCo_{1-x}Mn_xCl_3\cdot 2H_2O$.

To this end 10 samples of $(CH_3)_3NHCo_{1-x}Cu_xCl_3\cdot 2H_2O$ were measured with $x=0.039$ (5 samples), 0.058 (1 sample), 0.156 (1 sample), and 0.222 (3 samples); but in the area 18–58 GHz, 0–7 T, not a trace of these Cu^{2+} resonances could be found. Even with the very sensitive 35-GHz spectrometer we did not succeed to detect Cu^{2+} resonances. Therefore we are rather convinced that there are no Cu^{2+} resonances in the stated area, which suggests that the exchange coupling between the Cu^{2+} impurity and his Co^{2+} neighbors is so strong that it cannot be broken by the microwave energies and magnetic fields we use.

V. SPIN-CLUSTER RESONANCE (SCR)

The lines IV in Fig. 3 and the two low-field lines in Fig. 5 are resonances of the spin-cluster type; this type of resonance was first observed by Date *et al.*[11] in $CoCl_2\cdot 2H_2O$. Since then spin-cluster resonance has also been observed in $RbFeCl_3\cdot 2H_2O$,[12] $CsFeCl_3\cdot 2H_2O$,[22] and $Co(pyr)_2Cl_2$.[23]

A spin-cluster $|m\rangle$ is defined as a cluster of m adjacent spins in a chainlike compound reversed with respect to their position in the ground state. Given a set of local interchain exchange parameters J_i the excitation spectrum of a quasi-one-dimensional Ising

system with intrachain exchange J can be written

$$E_m = 2|J| + m\sum_i \alpha_i J_i + m\vec{\mu}\cdot\vec{H} \ , \quad (4)$$

where α_i contains information on the specific local magnetic array and m denotes the number of moments involved in the transition. Since the intrachain exchange interaction in $(CH_3)_3NHCoCl_3\cdot 2H_2O$ amounts to $J/k = 15.4$ K, the excitation spectrum in this case lies at least 21.4 cm^{-1} above the ground state and at low temperatures no transitions can be observed in the microwave range. However, when the temperature is increased spin clusters will be thermally excited and transitions that change the size of such a spin cluster (spin-cluster resonance) may be induced by microwave irradiation.

The general equation for spin-cluster resonance takes the form

$$h\nu = n(\Delta E + 2\vec{\mu}\cdot\vec{H}) \ , \quad (5)$$

where ΔE is some linear combination of interchain interaction parameters and n denotes the number of spins by which the spin cluster is changed in length. ΔE depends on the local environment of the excited spins and in the case of $\vec{H} \| c$,

$$\Delta E = 4J_2 + 2J_1 \ . \quad (6)$$

Here J_2 and J_1 are interaction parameters that are composed of exchange as well as dipolar contributions. J_1 is the interaction that couples the spins into layers in the b-c plane and J_2 is the interlayer interaction, as indicated in Fig. 2(a). The ΔE in formula (5) is given by formula (6) only when $\vec{H}$ in (4) and (5) is the sum of the applied and demagnetizing field. In practice, however, we use $h\nu = n(\Delta\tilde{E} + 2\vec{\mu}\cdot\vec{H})$ with $\vec{H}$ being the applied field. ΔE is then obtained from $\Delta\tilde{E}$ through a correction for the demagnetizing field.

The dashed lines in Fig. 3 are the lines $h\nu = \Delta\tilde{E} + 2\mu_c H (n=1)$ and $h\nu = 2(\Delta\tilde{E} + 2\mu_c H)(n=2)$ with $\Delta\tilde{E}/k = 0.241$ K and $\mu_c = 3.35\mu_B$ which corresponds to a g value of $g_c = 6.70$ in the $s = \frac{1}{2}$ fictitious spin formalism.

The lines through the spin-cluster resonance data of Fig. 5 are simply curves of the form $H = H_0/\cos\theta$, which behavior is expected in case of an Ising system where only the component of $\vec{H}$ along the moments plays a role. At increasing angles there is a deviation from the $1/\cos\theta$ behavior, indicating that the system is not perfectly Ising.

Knowing the spin configuration of the antiferromagnetic ground state as well as the ferromagnetic state, one can deduce by the method of Kudō and Katsura[24] some restrictions imposed on the interaction parameters. Thus we deduce $\mu_c H_{crit} = -2J_2$, $J_2 < 0$, and $J_1 > 0$. If we take H_{crit} to be 64 Oe,[18] J_2 takes on the value $J_2/k = -0.007$ K. Estimating the demagnetizing field to be approximately 0.5 kOe then the value of ΔE becomes $\Delta E/k = 0.47$ K and J_1 follows from $2J_1 = \Delta E - 4J_2$ as $J_1/k = 0.25$ K. If we now use Onsager's formula[25] for a rectangular Ising array $\sinh(J/kT_n)\sinh(J_1/kT_N) = 1$, with $T_N = 4.18$ K (Ref. 19) and $J_1/k = 0.25$ K then J follows as $J/k = 14.7$ K. This value for J is in good agreement with those obtained by Losee *et al.*[13] (15.4 K) and Groenendijk *et al.*[19] (13.3 K).

VI. DISCUSSION

Torque measurements by Yamamoto *et al.*[26] on $(CH_3)_3NHMnCl_3\cdot 2H_2O$ revealed a D value of -0.103 cm^{-1} and an E value of -0.034 cm^{-1}, and as $(CH_3)_3NHCoCl_3\cdot 2H_2O$ is isomorphous with $(CH_3)_3NHMnCl_3\cdot 2H_2O$ we expect roughly the same D and E values for Mn^{2+} in $(CH_3)_3NHCo_{1-x}Mn_xCl_3\cdot 2H_2O$. Comparison of these values with the experimental values in this case, $D = -0.128$ cm^{-1} and $E = -0.009$ cm^{-1}, indeed answers this expectation. A D value of comparable magnitude (-0.13 cm^{-1}) was observed by Fujii *et al.*[7] for Mn^{2+} in $Co_{1-x}Mn_xCl_2\cdot 2H_2O$. As shown by Yamamoto *et al.*[26] these large D values are not incidental but occur frequently when a Mn^{2+} is surrounded by an octahedron with two water molecules along the axial direction and four halogenide ions in the basal plane, especially the value $D = -0.370$ cm^{-1} for both $Cs_2MnBr_4\cdot 2H_2O$ and $Rb_2MnBr_4\cdot 2H_2O$ is the largest one reported up to date.[27]

So we might conclude that the anisotropy we measured originates from crystal-field effects. However, we may not conceal that there may be contributions to D and E arising from a mechanism of nondiagonal exchange as proposed by Tachiki[28] in order to account for the D value (-0.13 cm^{-1}) of Mn^{2+} in $Co_{1-x}Mn_xCl_2\cdot 2H_2O$. Tachiki assumed an exchange of the most general form $-2\vec{s}\cdot\vec{J}\cdot\vec{S}$ (7) where $\vec{s}$ is the cobalt spin and $\vec{S}$ denotes the manganese spin. Then using symmetry arguments and a second-order perturbation approach he showed that nondiagonal exchange between Co^{2+} and Mn^{2+} can give rise to a negative contribution to the D parameter in the manganese spin Hamiltonian. We shall not invoke this rather complicated mechanism because it introduces a lot of extra parameters that cannot be reduced by symmetry arguments as in the case of $Co_{1-x}Mn_xCl_2\cdot 2H_2O$. However, the observed internal field $\vec{H}_{int}$ must originate from exchange interactions between Mn^{2+} and Co^{2+}. It is easy to see that in a first-order perturbation approach the Hamiltonian (7) gives rise to a contribution in the manganese spin Hamiltonian of the form $J_{zx}S_x + J_{zy}S_y + J_{zz}S_z$ and comparison with the Hamiltonian (3) then shows that

$$J_{zx} = g_\perp\mu_B H^x_{int} \ , \quad J_{xy} = g_\perp\mu_B H^y_{int} \ , \quad J_{zz} = g_\parallel\mu_B H^z_{int} \ .$$

Then it follows from inserting $\vec{H}_{int}$ in these formulas that $J_{zx} \approx 0$, $J_{xz} \approx 0$, and $J_{zy}/k \approx 0.6$ K. So the only exchange tensor component that plays a role of importance is J_{zy} which couples the y component of the impurity spin to the z components of its left and right neighbor spin in the chain. This effective exchange that a Mn^{2+} experiences from its cobaltous surroundings in $(CH_3)_3NHCo_{1-x}Mn_xCl_3 \cdot 2H_2O$ is quite small, even smaller than that of a Mn^{2+} in $Co_{1-x}Mn_xCl_2 \cdot 2H_2O$.[7] We note that, though in several mixed systems the relation $J_{IH} = (J_{HH}J_{II})^{1/2}$ is obeyed,[29] it does not seem to work in our case for inserting $J_{HH}/k = 15.4$ K (Ref. 13) and $J_{II}/k = 0.36$ K (Ref. 15), we get $J_{IH}/k = 2.4$ K which is certainly in disagreement with the experimental results.

The spin-cluster resonance once more proved to be a valuable tool in determining the local interchain interaction parameters. The results from the SCR (g_c and ΔE) are in agreement with earlier results[13,18,19] obtained by other methods and corroborate the rectangular Ising character of $(CH_3)_3NHCoCl_3 \cdot 2H_2O$.

VII. CONCLUSION

Impurity spin resonance of Mn in $(CH_3)_3NHCo_{1-x}Mn_xCl_3 \cdot 2H_2O$ shows that the exchange between Mn^{2+} and Co^{2+} is small (that is, much smaller than the cobalt-cobalt intrachain exchange) and nondiagonal; in metaphorical language we may say that the Mn^{2+} impurities quite effectively break the Co^{2+} chains. On the other hand the absence of impurity spin resonance of Cu^{2+} in $(CH_3)_3NHCo_{1-x}Cu_xCl_3 \cdot 2H_2O$ suggests that the exchange between Cu^{2+} and Co^{2+} is considerable, therefore it may be worthwhile to look for these resonances at higher frequencies (e.g., far infrared).

Hence our resonance experiments affirm the assumption of Takeda and Schouten that the manganese impurities act as weakly magnetic impurities, whereas the experiments are inconclusive as to the "magnetic strength" of the copper impurities.

ACKNOWLEDGMENTS

The authors gratefully acknowledge the financial support of the Stichting voor Fundamenteel Onderzoek der Materie (FOM) that forms part of the Netherlands Organization for the Advancement of Pure Research. We also are indebted to H. Hadders for preparing the single crystals.

[1]For a review see, for instance, J. C. Schouten, Ph.D. thesis (Eindhoven, 1981) (unpublished).
[2]D. Hone, P. A. Montano, T. Tonegawa, and Y. Imry, Phys. Rev. B 12, 5141 (1975).
[3]K. Takeda, J. Phys. Soc. Jpn. 40, 1781 (1976); K. Takeda and J. C. Schouten, *ibid.* 50, 2554 (1981).
[4]J. C. Schouten, K. Takeda, and K. Kopinga, J. Phys. C 6, 723 (1978).
[5]M. Date and M. Motokawa, Phys. Rev. Lett. 15, 854 (1965).
[6]M. Motokawa and M. Date, J. Phys. Soc. Jpn. 23, 1216 (1967).
[7]N. Fujii, M. Motokawa, and M. Date, J. Phys. Soc. Jpn. 25, 700 (1968).
[8]L. L. Chase and H. J. Guggenheim, Phys. Lett. 28A, 694 (1969).
[9]G. Mischler, P. Carrara, and Y. Merle D'Aubigné, Phys. Rev. B 15, 1568 (1977).
[10]J. Tuchendler, J. Magariño, D. Bertrand, and A. R. Fert, J. Phys. C 13, 233 (1980).
[11]M. Date and M. Motokawa, Phys. Rev. Lett. 16, 1111 (1966).
[12]Q. A. G. van Vlimmeren and W. J. M. de Jonge, Phys. Rev. B 19, 1503 (1979); Q. A. G. van Vlimmeren, Ph.D. thesis (Eindhoven, 1979) (unpublished).
[13]D. B. Losee, J. N. McElearney, G. E. Shankle, R. L. Carlin, P. J. Cresswell, and W. T. Robinson, Phys. Rev. B 8, 2185 (1973).
[14]D. B. Losee, J. N. McElearny, A. Siegel, R. L. Carlin, A. A. Khan, J. P. Roux, and W. J. James, Phys. Rev. B 6, 4342 (1972).
[15]S. Merchant, J. N. McElearney, G. E. Shankle, and R. L. Carlin, Physica (Utrecht) 78, 308 (1974).
[16]R. E. Caputo, R. D. Willett, and J. A. Muir, Acta Crystallogr. Sect. B 32, 2639 (1976).
[17]H. A. Algra, L. J. de Jongh, W. J. Huiskamp, and R. L. Carlin, Physica (Utrecht) 92B, 187 (1977).
[18]R. D. Spence and A. C. Botterman, Phys. Rev. B 9, 2993 (1974).
[19]H. A. Groenendijk and A. J. van Duyneveldt, J. Magn. Magn. Mater. 15–18, 1032 (1980).
[20]Q. A. G. van Vlimmeren, Ph.D. thesis (Eindhoven, 1979) (unpublished).
[21]B. Bleaney and K. W. H. Stevens, Rep. Prog. Phys. 16, 108 (1953).
[22]A. C. Phaff and I. J. M. M. Raaymakers (unpublished).
[23]C. H. W. Swüste, A. C. Phaff, and W. J. M. de Jonge, J. Chem. Phys. 73, 4646 (1980).
[24]T. Kudō and S. Katsura, Prog. Theor. Phys. 56, 435 (1976).
[25]L. Onsager, Phys. Rev. 65, 117 (1944).
[26]I. Yamamoto, K. Iio, and K. Nagata, J. Phys. Soc. Jpn. 49, 1756 (1980).
[27]C. H. W. Swüste, Ph.D. thesis (Eindhoven, 1973) (unpublished).
[28]M. Tachiki, J. Phys. Soc. Jpn. 25, 686 (1968).
[29]R. A. Cowley and W. J. L. Buyers, Rev. Mod. Phys. 44, 406 (1972).